

Optimal Trading of a Charging-Station Company in Auction Markets for Electricity

Farnaz Sohrabi, Mohammad Rohaninejad, Mohammad Reza Hesamzadeh, *Senior Member, IEEE*, Július Bemš

Abstract—This paper addresses a charging-station company (Chargco) for electric and hydrogen vehicles. The optimal trading of the Chargco in day-ahead and intraday auction markets for electricity is modeled as a stochastic Mixed-Integer Quadratic Program (MIQP). We propose a series of linearization and reformulation techniques to reformulate the stochastic MIQP as a mixed-integer linear program (MILP). To model stochasticity, we utilize generative adversarial networks to cluster electricity market price scenarios. Additionally, a combination of random forests and linear regression is employed to model the relationship between Chargco electricity and hydrogen loads and their selling prices. Finally, we propose an Improved L-Shaped Decomposition (ILSD) algorithm to solve our stochastic MILP. Our ILSD algorithm not only addresses infeasibilities through an innovative approach but also incorporates warm starts, valid inequalities and multiple generation cuts, thereby reducing computational complexity. Numerical experiments illustrate the Chargco trading using our proposed stochastic MILP and its solution algorithm.

Index Terms—L-shaped decomposition, Charging station, Electricity auction markets, Generative adversarial networks (GANs), Random forest, Stochastic programming.

NOMENCLATURE

Indices

ω	Index for scenarios.
ω_1, ω_2	Index for day-ahead and intraday scenarios.
j	Index for bidding price steps.
t', t	Index for day-ahead and intraday intervals.

Constants

η^b, η^h, η^e	Efficiency of battery, tank, and electrolyzer.
H	Heating value of hydrogen.
π_ω	Probabilities associated with scenarios.
$\underline{b}^c, \bar{b}^c$	Min and max for battery charging capacity. ¹
$\underline{b}^d, \bar{b}^d$	Min and max for battery discharging capacity.
$\underline{b}^l, \bar{b}^l$	Min and max for battery level capacity.
$\underline{e}^p, \bar{e}^p$	Min and max for electrolyzer capacity.
$\underline{h}^c, \bar{h}^c$	Min and max for tank charging capacity.
$\underline{h}^d, \bar{h}^d$	Min and max for tank discharging capacity.
$\underline{h}^l, \bar{h}^l$	Min and max for tank capacity.
$\xi_{t'\omega_1}^d, \xi_{t\omega_2}^i$	Day-ahead and intraday electricity prices.
y_j	Electricity bidding price steps.

Variables

$b_{t\omega}^c, b_{t\omega}^d$	Charged and discharged power from battery.
$b_{t\omega}^l, h_{t\omega}^l$	Power and hydrogen level in battery and tank.
$e_{t\omega}^p$	Consumed power by electrolyzer.
$h_{t\omega}^c, h_{t\omega}^d$	Charged and discharged hydrogen from tank.
l_t^e, l_t^h	Electricity and hydrogen loads.
$m_{t\omega_1}^d, m_{t\omega_2}^i$	Day-ahead and intraday bought power.

p_t^e, p_t^h	Electricity and hydrogen selling prices.
$u_{t\omega}^b, u_{t\omega}^h$	Operation mode for battery and tank.
$v_{t\omega}^e, v_{t\omega}^h$	Dedicated electricity and hydrogen for loads.
$x_{jt'}^d, x_{jt\omega_1}^i$	Bid volume in day-ahead and intraday markets.

I. INTRODUCTION

THE use of fossil fuels has a negative effect on the environment and depletes these resources [1]. Transportation accounts for roughly 20% of global CO₂ emissions, with three-quarters of this attributed to road transport [2]. This has led to a growing interest in battery electric and hydrogen fuel cell vehicles as environmentally friendly alternatives [3]. As a result, innovative solutions such as combined electric and hydrogen charging stations are emerging to meet the growing demand for sustainable transportation. However, research on these systems is still limited, creating a significant gap in our understanding, particularly regarding their participation in electricity markets. It is essential to explore how these stations can effectively engage in electricity markets, develop effective solution methods, and manage the uncertainties that arise in this context. This paper addresses these challenges by investigating strategies for integrating these stations into the energy market. We focus on key aspects, including mathematical modeling, linearization techniques, and the implementation of adaptable algorithms capable of responding to the dynamic nature of energy trading and the associated uncertainties.

A. Literature review

Authors in [4] propose a day-ahead optimization framework for sustainable energy supply to an electric and hydrogen vehicle refueling station, utilizing a hybrid multi-objective strategy to handle uncertainties. Similarly, Panah et al. [5] tackle the challenge of developing a charging station that meets both hydrogen and electricity needs, serving public transportation systems alongside private vehicles. In off-grid areas, Xu et al. [6] exclusively rely on solar photovoltaics for electric vehicle charging and hydrogen refueling. The optimization of a multi-product charging station that utilizes a combination of the rolling planning method, scenario reduction, and sample average approximation is presented in [7]. An on-grid station is proposed in [8] to support hydrogen and electric vehicles, incorporating a hybrid stochastic and distributionally robust optimization method to address uncertainties in energy management. Reference [9] presents an autonomous hybrid charging station powered by a photovoltaic system for charging hydrogen and electric vehicles, addressing inherent demand uncertainties using information-gap decision

¹Min: minimum, Max.: Maximum

theory (IGDT). A real-time energy management strategy for intelligent solar parking lots that charge both electric and hydrogen vehicles is presented in [10], addressing challenges posed by uncertainties through a deep reinforcement learning model. Elmasry et al. present an integrated electricity-hydrogen system with multi-level hydrogen storage and solar PV that supplies electric and fuel cell vehicles at three charging points: an electric vehicle station, a fuel cell car refueling station, and a fuel cell truck refueling station, with the cost function representing daily energy costs [11]. In reference [12], a bi-level coordination optimization model is introduced for an integrated energy system and a hybrid charging station, with the aim of maximizing social benefits while meeting the energy requirements of environmentally friendly vehicles for both electricity and hydrogen. The energy needs of an off-grid refueling station for electric and hydrogen vehicles, along with a temporary residence, are designed and analyzed in [13] using renewable energy sources such as wind and solar power. A low-carbon energy management model for a microgrid that integrates hydrogen, heat, and power systems, incorporating charging stations to simultaneously meet the energy needs of both hydrogen and electric vehicles, is presented in [14]. An economically optimal energy management model for a charging station that utilizes a photovoltaic system and an electrolyzer to charge both electric and hydrogen vehicles is proposed in [15], employing a mixed-integer linear programming approach. In [16], a grid-connected photovoltaic system for charging electric vehicles and refueling fuel cell vehicles was examined through numerical simulations and optimized using a genetic algorithm to identify cost-effective component sizes and energy management strategies.

The existing literature has not thoroughly examined the trading activities of charging station owners in electricity markets, presenting a significant research gap. While various studies have explored the optimization and operational strategies of charging stations, the specific dynamics of how charging station owners engage in electricity trading remain largely unexplored. This oversight limits our understanding of the potential economic benefits and challenges that charging station operators may face in these markets. As the electrification of transport systems continues to evolve, it is crucial to investigate how these stakeholders can effectively participate in electricity trading to enhance their profitability and sustainability. Addressing this gap will provide valuable insights into the strategic decisions of charging station owners, potentially leading to more robust frameworks that support the energy transition.

As innovative charging station solutions gain attention, understanding their integration into the electricity markets becomes crucial. The European energy exchange introduced diverse trading opportunities, spanning futures, spot, and balancing markets. Our focus is on the spot market, renowned for its prominence in the energy landscape [17]. In most European countries, the spot market encompasses both day-ahead and intraday markets [18]. We focus on discrete-auction mechanisms, which entails buying and selling power one day or several hours in advance to meet the real-time demand.

Generative Adversarial Networks (GANs) can be utilized

for clustering electricity market price scenarios from historical data without the need for explicit model specifications. It utilizes unsupervised learning to eliminate the need for time-consuming manual labeling, which is particularly impractical for large datasets [19]. The GANs, developed by Goodfellow et al. [20], consist of two neural networks engaged in a competitive game. The generator produces synthetic samples from a training dataset, while the discriminator distinguishes between fake and real samples.

The random forest method is categorized as an ensemble method, combining multiple classifiers into a single system. It achieves higher classification accuracy than any individual classifier that could attain alone [21]. The main advantage of the random forest method is its independence from prior knowledge regarding the data distribution [22]. The random forest uses multiple decision trees to reduce errors. It involves randomly selecting training instances, choosing feature subsets to split nodes, and learning from random samples during training [23].

In discrete optimization, stochastic Mixed-Integer Linear Programs (MILPs) cause significant challenges due to increasing memory requirements and computational workload with scenario growth. Various decomposition techniques have been developed to address this issue by breaking down complex stochastic MILP problems into more manageable sub-problems. L-shaped decomposition is one such technique that estimates the expected second-stage recourse function through optimality cuts in the first stage, employing dual solutions from the second-stage problems. This iterative process between a master problem and a sub-problem exchanges information to derive the optimal solution [24].

Another complexity in this study arises from the time-decoupled framework. The problem addressed spans 24 hours, and due to intrinsic time coupling in the constraints of energy storage, it cannot be solved independently for each time period. This is consistent with findings in the literature, such as those by Derakhshandeh et al. [25], who discuss the challenges of time coupling in energy management.

B. Contributions

The contributions of the current paper are as follows:

First, we develop a two-stage stochastic Mixed-Integer Quadratic Program (MIQP) for optimal trading of a charging-station company (Chargco) in Day-Ahead (DA) and Intraday (ID) markets. A series of linearization techniques is applied to approximate the MIQP as a MILP. This includes piecewise linearization method utilizing special ordered sets of type 2 (SOS2) variables and max-affine functions.

Second, we develop a surrogate model incorporating random forest and linear regression to enhance the model's ability to predict electricity and hydrogen load levels, along with their corresponding prices.

Third, To address challenges related to scenario reduction, we utilize GANs on annual real electricity market prices. The GANs is utilized to cluster scenarios, effectively representing uncertainties in both DA and ID electricity prices.

Fourth, the approximated MILP is solved using an Improved L-Shaped Decomposition (ILSD) algorithm. The orig-

inal MILP is broken down into a Master Problem (MP) that optimizes hydrogen and electricity load levels, selling prices, and day-ahead bidding, followed by a Sub-Problem (SP) for intraday bidding and device operations. We demonstrate in **Lemma 1** that the SP can be reformulated as an equivalent LP. Additionally, our ILSD algorithm eliminates the need for feasibility cuts or slack variables, as shown in **Lemma 2**. The algorithm is further enhanced by warm-start techniques, valid inequalities, and multiple-cuts generation to reduce computational complexities. The effectiveness of the MILP model and solution algorithm is illustrated through a case study, providing valuable insights for electricity market decision-making.

The paper is structured as follows: Section II formulates the stochastic MILP for Chargco optimal trading and explains the random forest method. Scenario generation using GANs is detailed in Section III. The improved L-shaped decomposition algorithm is discussed in Section IV, followed by the case study in Section V. Finally, Section VI concludes the paper.

II. PROFIT-MAXIMIZING CHARGING-STATION COMPANY FOR ELECTRIC AND HYDROGEN VEHICLES

We consider a profit-maximizing charging-station company owning electric and hydrogen vehicle charging stations. Chargco submits bids to DA and ID markets, purchasing electricity for Electric Charging Stations (ECSs) and Hydrogen Charging Stations (HCSs), as shown in Fig. 1. The purchased electricity serves three purposes: direct electric vehicle charging, charging battery storage, and hydrogen production via the electrolyzer, for storage or direct hydrogen vehicle charging.

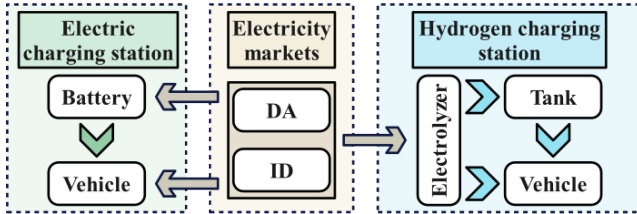


Fig. 1. The Chargco owning ECSs and HCSs participating in markets

Chargco participates in sequential DA and ID markets, as depicted in Fig. 2. DA market operates hourly, while ID market operates quarter-hourly². Chargco optimizes 24 bid curves for the DA market (one per hour) and 96 bid curves for the ID market (one per quarter) to maximize profit.

The Chargco's profit-maximizing problem is structured as a two-stage stochastic optimization problem, depicted in Fig. 3. The first stage involves formulating DA bidding decisions, while the second stage constructs ID bidding curves and schedules equipment operations. This approach explicitly models the impact of ID bids on the DA bids and vice versa.

A. Mixed-Integer Quadratic Program (MIQP) formulation

In this section, we formulate the MIQP model for Chargco's profit-maximization problem over a single day. The objective

²European ID auctions' market time unit (MTU) varies: hourly in Switzerland, half-hourly in France, and quarter-hourly in Germany, Austria, Belgium, and the Netherlands [26].

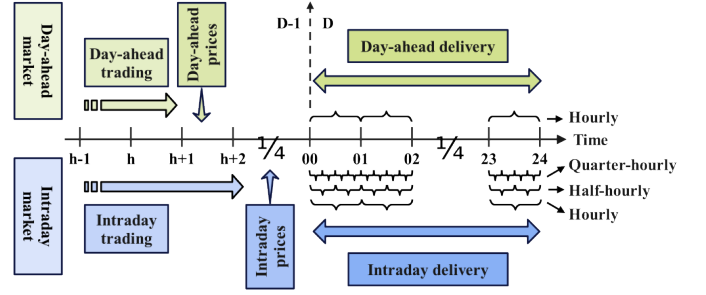


Fig. 2. The sequence of events in the DA and ID markets.

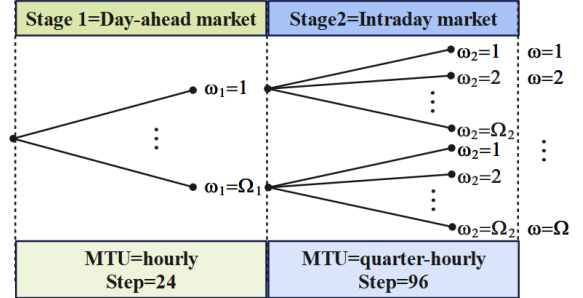


Fig. 3. Two-stage stochastic optimization problem.

function, defined in Eq. (1), seeks to maximize Chargco's total profit. This profit is defined by calculating the costs of purchasing electricity from both the DA and ID markets from the revenue earned by selling electricity and hydrogen to vehicles. In this formulation, t represents the time index for the DA market with hourly intervals, and t' represents the time index for the ID market with quarter-hourly intervals.

$$\begin{aligned} \text{maximize}_{\Xi} & \left[\sum_t (l_t^e p_t^e + l_t^h p_t^h) - \sum_{t', t \in t', \omega, (\omega_1, \omega_2) \in \omega} \pi_\omega (m_{t\omega_1}^d \xi_{t'\omega_1}^d + m_{t\omega}^i \xi_{t'\omega}^i) \right] \\ \Xi = & [l_t^e, p_t^e, l_t^h, p_t^h, m_{t\omega_1}^d, m_{t\omega}^i, v_{t\omega}^e, v_{t\omega}^h, b_{t\omega}^c, b_{t\omega}^d, b_{t\omega}^l, e_{t\omega}^p, \\ & h_{t\omega}^c, h_{t\omega}^d, h_{t\omega}^l, x_{jt'}^d, x_{jt\omega_1}^i, u_{t\omega}^b, u_{t\omega}^h] \end{aligned} \quad (1)$$

Equation (2) ensures that the combined power purchased from both the DA and ID markets matches the electricity allocated for electric vehicle charging, battery charging, and electrolyzer consumption.

$$m_{t\omega_1}^d + m_{t\omega}^i = v_{t\omega}^e + b_{t\omega}^c + e_{t\omega}^p \quad \forall t, \forall \omega, \forall \omega_1 \in \omega \quad (2)$$

Equation (3a) represents the power balance of the battery. Constraints (3b)-(3d) set limits on the battery's inventory level, charging capacity, and discharging capacity, respectively.

$$b_{t\omega}^l = b_{t-1, \omega}^l + \eta^b b_{t\omega}^c - b_{t\omega}^d / \eta^b : \tau_{t\omega} \quad \forall t, \forall \omega \quad (3a)$$

$$b_{t\omega}^l \leq b_{t\omega}^l \leq \bar{b}^l \quad \forall t, \forall \omega \quad (3b)$$

$$b_{t\omega}^c u_{t\omega}^b \leq b_{t\omega}^c \leq \bar{b}^c u_{t\omega}^b : \underline{\tau}_{t\omega}^c, \bar{\tau}_{t\omega}^c \quad \forall t, \forall \omega \quad (3c)$$

$$b_{t\omega}^d (1 - u_{t\omega}^b) \leq b_{t\omega}^d \leq \bar{b}^d (1 - u_{t\omega}^b) : \underline{\tau}_{t\omega}^d, \bar{\tau}_{t\omega}^d \quad \forall t, \forall \omega \quad (3d)$$

Equation (4a) aligns produced hydrogen with tank charging and vehicle refueling. Constraint (4b) restricts electrolyzer power consumption.

$$\eta^e e_{t\omega}^p / H = h_{t\omega}^c + v_{t\omega}^h \quad \forall t, \forall \omega \quad (4a)$$

$$\underline{e}^p \leq e_{t\omega}^p \leq \bar{e}^p \quad \forall t, \forall \omega \quad (4b)$$

Equation (5a) outlines hydrogen balance in the tank. Constraints (5b) to (5d) limit inventory, charging, and discharging capacity.

$$h_{t\omega}^l = h_{t-1,\omega}^l + \eta^h h_{t\omega}^c - h_{t\omega}^d / \eta^h : \nu_{t\omega} \quad \forall t, \forall \omega \quad (5a)$$

$$\underline{h}^l \leq h_{t\omega}^l \leq \bar{h}^l \quad \forall t, \forall \omega \quad (5b)$$

$$\underline{h}^c u_{t\omega}^h \leq h_{t\omega}^c \leq \bar{h}^c u_{t\omega}^h : \underline{\nu}_{t\omega}^c, \bar{\nu}_{t\omega}^c \quad \forall t, \forall \omega \quad (5c)$$

$$\underline{h}^d (1 - u_{t\omega}^h) \leq h_{t\omega}^d \leq \bar{h}^d (1 - u_{t\omega}^h) : \underline{\nu}_{t\omega}^d, \bar{\nu}_{t\omega}^d \quad \forall t, \forall \omega \quad (5d)$$

Equation (6a) states the electric vehicle load equals the sum of power purchased and discharged from the battery, while (6b) ensures hydrogen supplied from the electrolyzer and released from the tank meets hydrogen demand.

$$v_{t\omega}^e + b_{t\omega}^d = l_t^e \quad \forall t, \forall \omega \quad (6a)$$

$$v_{t\omega}^h + h_{t\omega}^d = l_t^h \quad \forall t, \forall \omega \quad (6b)$$

Equation (7a) specifies DA market bidding curves using a piece-wise linear model, while constraint (7b) ensures their non-increasing nature according to market rules.

$$\sum_{t \in t'} m_{t\omega_1}^d = \frac{\xi_{t'\omega_1}^d - y_j}{y_{j+1} - y_j} x_{j+1,t'}^d + \frac{y_{j+1} - \xi_{t'\omega_1}^d}{y_{j+1} - y_j} x_{j,t'}^d \quad (7a)$$

$$\text{if } y_j \leq \xi_{t'\omega_1}^d < y_{j+1} \quad \forall t', \forall \omega_1, \forall j \in \{1, \dots, J-1\} \quad (7a)$$

$$x_{j+1,t'}^d \leq x_{j,t'}^d \quad \forall t', \forall j \in \{1, \dots, J-1\} \quad (7b)$$

Equation (8a) specifies ID market bidding curves, while constraint (8b) ensures their non-increasing nature, based on observed DA market outcomes.

$$m_{t\omega}^i = \frac{\xi_{t\omega_2}^i - y_j}{y_{j+1} - y_j} x_{j+1,t\omega_1}^i + \frac{y_{j+1} - \xi_{t\omega_2}^i}{y_{j+1} - y_j} x_{j,t\omega_1}^i \quad (8a)$$

$$\text{if } y_j \leq \xi_{t\omega_2}^i < y_{j+1} \quad \forall t, \forall \omega, (\omega_1, \omega_2) \in \omega \quad (8a)$$

$$\forall j \in \{1, \dots, J-1\} \quad (8a)$$

$$x_{j+1,t\omega_1}^i \leq x_{j,t\omega_1}^i \quad \forall t, \forall \omega_1, \forall j \in \{1, \dots, J-1\} \quad (8b)$$

We approximate our non-linear function using line segments and constraints to determine the active segment. Binary variable u_{tm} indicates the active segment, while \underline{p}_{tm} and \bar{p}_{tm} bound the price. Equation (9c) ensures only one segment is active per t , and (9d) expresses the linear relationship between l_t and p_t within the segment. Parameters are obtained from machine learning, and M is a large positive constant.

$$\underline{p}_{tm} - (1 - u_{tm}) M \leq p_t \quad \forall t, \forall m \quad (9a)$$

$$p_t \leq \bar{p}_{tm} + (1 - u_{tm}) M \quad \forall t, \forall m \quad (9b)$$

$$\sum_m u_{tm} = 1 \quad \forall t \quad (9c)$$

$$l_t \leq A_{tm} p_t + B_{tm} + (1 - u_{tm}) M \quad \forall t, \forall m \quad (9d)$$

In our study, we employ random forest as a surrogate model to capture the relationship between electricity and hydrogen load levels and their selling prices efficiently. Random forest employs bootstrap aggregating to train decision trees on B random subsets of the data with replacement, utilizing feature bagging during construction. Predictions for new samples x' are made by averaging predictions from all individual trees f_b [27], as represented by Equation (10):

$$\hat{f} = \frac{1}{B} \sum_{b=1}^B f_b(x') \quad (10)$$

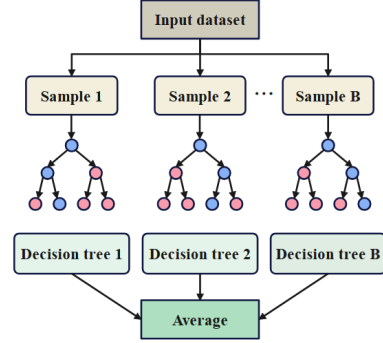


Fig. 4. Schematic diagram of the random forest algorithm.

The decision variables for the problem are outlined in (11a) and (11b). Lagrange multipliers, corresponding to each constraint, are separated by colons.

$$u_{t\omega}^b, u_{t\omega}^h \in \{0, 1\} \quad (11a)$$

$$l_t^e, p_t^e, l_t^h, p_t^h, m_{t\omega_1}^i, m_{t\omega}^i, v_{t\omega}^e, v_{t\omega}^h, b_{t\omega}^c, b_{t\omega}^d, b_{t\omega}^l, e_{t\omega}^p, \quad (11b)$$

$$h_{t\omega}^c, h_{t\omega}^d, h_{t\omega}^l, x_{j,t'}^d, x_{j,t\omega_1}^i \in \mathbb{R} \quad (11b)$$

The derived MIQP is set out below:

$$\text{maximize } (1) \quad (12a)$$

$$\text{Subject to : } (2) - (11b) \quad (12b)$$

B. Converting MIQP (1) to a MILP

For the bilinear terms $l_t^e p_t^e$ and $l_t^h p_t^h$ in objective function (1), we use a piecewise linearization technique with SOS2 variables and a max-affine function. Using SOS2 variables is a well-established method for approximating nonlinear functions through a series of line segments. In this approach, only two consecutive variables from the set can take non-zero values, enabling smooth interpolation between predefined breakpoints. This transforms the original objective function (1) to a modified form (13).

$$\text{maximize } \left[\sum_t (w_{1t}^e - w_{2t}^e + w_{1t}^h - w_{2t}^h) - \sum_{t', t \in t', \omega, (\omega_1, \omega_2) \in \omega} \pi_\omega (m_{t\omega_1}^d \xi_{t'\omega_1}^d + m_{t\omega}^i \xi_{t\omega_2}^i) \right] \quad (13)$$

Since the linearization procedure for both bilinear terms is the same, we express it once as written in (14a)-(16) without superscript e and h . The calculation of w_{1t} and w_{2t} is shown

in (14a). (14b) demonstrates that the difference between w_{1t} and w_{2t} is equal to the product of l_t and p_t .

$$w_{1t} = (0.5(l_t + p_t))^2, w_{2t} = (0.5(l_t - p_t))^2 \quad \forall t \quad (14a)$$

$$w_{1t} - w_{2t} = l_t p_t \quad \forall t \quad (14b)$$

1) *Linearization of $(0.5(l_t + p_t))^2$* : In equations (15a)-(15e), we compute w_{1t} . Equation (15a) determines the interval size for f_{tm} calculation based on $0.5(l_t + p_t)$ range. Equation (15b) computes m -th f_{tm} value. Equation (15c) represents l_t and p_t relationship, where β_{tm} is segment contribution. Equation (15d) calculates w_{1t} , and (15e) ensures β_{tm} sum equals 1 and are SOS2 type.

$$\text{interval}_{tm} = \frac{\max_{tm} - \min_{tm}}{M - 1} \quad (15a)$$

$$f_{tm} = \min_{tm} + m \times \text{interval}_{tm} \quad (15b)$$

$$0.5(l_t + p_t) = \sum_m \beta_{tm} f_{tm} \quad \forall t \quad (15c)$$

$$w_{1t} = \sum_m \beta_{tm} (f_{tm})^2 \quad \forall t \quad (15d)$$

$$\sum_m \beta_{tm} = 1, \beta_{tm} \in \text{SOS2} \quad \forall t \quad (15e)$$

2) *Linearization of $(0.5(l_t - p_t))^2$* : In equation (16), we describe the calculation of w_{2t} using a max-affine function. Here, we determine the interval size for computing f_{tm} based on the range between the maximum and minimum values of $0.5(l_t - p_t)$. Next, we obtain the coefficients a_{tm} and the constants b_{tm} for each line.

$$w_{2t} \geq 0.5(l_t - p_t) a_{tm} + b_{tm} \quad \forall t, m = 1, \dots, M - 1 \quad (16)$$

We prefer the max-affine function to linearize $(0.5(l_t - p_t))^2$ to avoid introducing SOS2 variables, which would complicate the problem. However, we can't use the max-affine function for $(0.5(l_t + p_t))^2$ linearization because we maximize a convex problem. The final stochastic MILP is presented below:

$$\text{maximize} \quad (13) \quad (17a)$$

$$\text{Subject to : } (2) - (11b), (9a) - (16) \quad (17b)$$

III. GENERATIVE ADVERSARIAL NETWORK

The MILP (17) is a stochastic two-stage optimization problem. We use GANs to cluster scenarios representing uncertainties in DA and ID electricity prices, refining this with the Interquartile Range (IQR) to remove outliers. The IQR identifies abnormal outliers beyond 1.5 times its value [28].

$$\text{IQR} : Q3 - Q1 \quad (18a)$$

$$\text{OU} > Q3 + 1.5 \times \text{IQR}, \text{OL} < Q1 - 1.5 \times \text{IQR} \quad (18b)$$

The GANs model (Fig. 5) consists of two neural networks: the generator $G(z; l^G)$ and the discriminator $D(x; l^D)$, with associated weights l^G and l^D . The generator uses random noise inputs z from distribution \mathbb{P}_z to produce scenarios until the discriminator cannot distinguish them from real historical samples x . The discriminator aims to differentiate between real data from \mathbb{P}_x and generated data from \mathbb{P}_z . Loss functions

L^G and L^D optimize the neural network weights, creating the min-max optimization model (19c). We employed the Keras backend [29] with TensorFlow [30] for GANs model development and training.

$$\min_{l^G} L^G = -\mathbb{E}_{z \sim \mathbb{P}_z} [\log(D(G(z; l^G); l^D))] \quad (19a)$$

$$\min_{l^D} L^D = -\mathbb{E}_{x \sim \mathbb{P}_x} [\log(D(x; l^D))] - \mathbb{E}_{z \sim \mathbb{P}_z} [\log(1 - D(G(z; l^G); l^D))] \quad (19b)$$

$$\min_{l^G} \max_{l^D} \mathbb{E}_{x \sim \mathbb{P}_x} [\log(D(x; l^D))] + \mathbb{E}_{z \sim \mathbb{P}_z} [\log(1 - D(G(z; l^G); l^D))] \quad (19c)$$

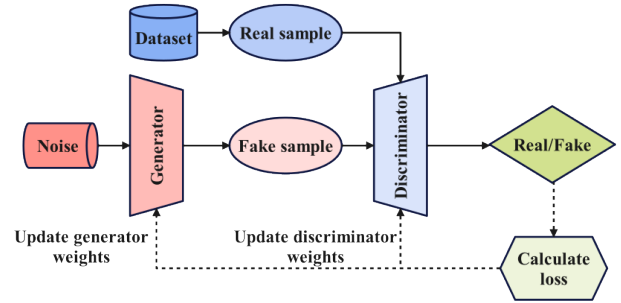


Fig. 5. Generative adversarial network structure.

The scenario number is optimal if the Mean Squared Error (MSE) between real and generated data falls below a threshold ϵ . Equation (20a) computes the MSE between observed (y_i) and predicted (\hat{y}_i) values with n data points [31]. As the exact Probability Density Function (PDF) is unknown, we estimate it using Kernel Density Estimation (KDE) due to discrete samples. Equation (20b) presents the kernel density estimate $\hat{f}(x)$ for a dataset $\{X_i\}$, where $K(\cdot)$ is the kernel function, h is the bandwidth, and n is the number of data points [32].

$$\text{MSE} = \frac{1}{n} \sum_{i=1}^n (y_i - \hat{y}_i)^2 \quad (20a)$$

$$\hat{f}(x) = \frac{1}{nh} \sum_{i=1}^n K\left(\frac{x - X_i}{h}\right) \quad (20b)$$

IV. THE IMPROVED L-SHAPED DECOMPOSITION (ILSD) ALGORITHM

Solving the MILP (17) is computationally challenging due to the interconnection of DA and ID markets and a large number of operational variables. To address this, we improve and employ the L-shaped decomposition algorithm, which decomposes the original MILP into MP and SP, iteratively solving them to find the optimal solution.³

A. The L-shaped decomposition Master Problem

The electricity and hydrogen load levels, their selling prices and DA power purchases are optimized in the L-shaped decomposition MP and then they are passed to the L-shaped

³In this paper, the optimal solution refers to an ϵ -optimal solution where ϵ is a small number indicating the optimality gap of the solution, defined as: $\epsilon = \frac{UB-LB}{UB}$.

decomposition SP. Optimality cut (21c) iteratively refines MP decisions with α underestimating the objective function of SP.

L-shaped decomposition MP:

$$\text{maximize}_{\Xi} \sum_t (w_{1t}^e - w_{2t}^e + w_{1t}^h - w_{2t}^h) - \quad (21a)$$

$$\sum_{t', t \in t', \omega, \omega_1 \in \omega} \pi_{\omega} (m_{t\omega_1}^d \xi_{t'\omega_1}^d) - \alpha$$

$$\Xi = [w_{1t}^e, w_{2t}^e, w_{1t}^h, w_{2t}^h, \beta_{tm}^e, \beta_{tm}^h, u_{tm}^e, u_{tm}^h, l_t^e, p_t^e, l_t^h, p_t^h, m_{t\omega_1}^d, x_{jt'}^d, \alpha]$$

$$\text{subject to : (7a), (7b), (9a) - (16)} \quad (21b)$$

$$\alpha \geq -\alpha (\hat{m}_{nt\omega_1}^d, \hat{l}_{nt}^e, \hat{l}_{nt}^h) + \sum_{t, \omega, \omega_1 \in \omega} [(\hat{m}_{nt\omega_1}^d - m_{t\omega_1}^d)]$$

$$\lambda_{nt\omega} + (\hat{l}_{nt}^e - l_t^e) \vartheta_{nt\omega} + (\hat{l}_{nt}^h - l_t^h) \varrho_{nt\omega} \quad \forall n, \quad (21c)$$

$$u_{tm}^e, u_{tm}^h \in \{0, 1\}, \beta_{tm}^e, \beta_{tm}^h \in \text{SOS2} \quad \forall t \quad (21d)$$

$$w_{1t}^e, w_{2t}^e, w_{1t}^h, w_{2t}^h, l_t^e, p_t^e, l_t^h, p_t^h, m_{t\omega_1}^d, x_{jt'}^d, \alpha \in \mathbb{R} \quad (21e)$$

B. The L-shaped decomposition Sub-problem

The L-shaped decomposition SP optimizes ID bidding curves and charging-station operation.

L-shaped decomposition SP:

$$\text{maximize}_{\Xi} \sum_{t, \omega, \omega_2 \in \omega} \pi_{\omega} (-m_{t\omega_2}^i \xi_{t\omega_2}^i) \quad (22a)$$

$$\Xi = [m_{t\omega}^i, v_{t\omega}^e, v_{t\omega}^h, b_{t\omega}^e, b_{t\omega}^d, b_{t\omega}^l, e_{t\omega}^p, h_{t\omega}^e, h_{t\omega}^d, h_{t\omega}^l, x_{jt\omega_1}^i, u_{t\omega}^b, u_{t\omega}^h]$$

$$\text{subject to : (3a) - (5d), (8a), (8b), (11a)} \quad (22b)$$

$$\hat{m}_{nt\omega_1}^d = v_{t\omega}^e + b_{t\omega}^c + e_{t\omega}^p - m_{t\omega}^i : \lambda_{nt\omega} \quad \forall n, \forall t, \quad (22c)$$

$$\forall \omega, \forall \omega_1 \in \omega$$

$$v_{t\omega}^e + b_{t\omega}^d = \hat{l}_{nt}^e : \vartheta_{nt\omega} \quad \forall n, \forall t, \forall \omega \quad (22d)$$

$$v_{t\omega}^h + h_{t\omega}^d = \hat{l}_{nt}^h : \varrho_{nt\omega} \quad \forall n, \forall t, \forall \omega \quad (22e)$$

$$m_{t\omega}^i, v_{t\omega}^e, v_{t\omega}^h, b_{t\omega}^c, b_{t\omega}^d, b_{t\omega}^l, e_{t\omega}^p, h_{t\omega}^e, h_{t\omega}^d, h_{t\omega}^l, x_{jt\omega_1}^i \in \mathbb{R} \quad (22f)$$

The binary variable $u_{t\omega}^b$ and $u_{t\omega}^h$, categorize the L-shaped decomposition SP as a MILP. Lemma 1 reformulates the MILP model of L-shaped decomposition SP as an equivalent LP.

Lemma 1. *If the binary variables in the L-shaped decomposition SP (22a)-(22f) are removed, the resulting relaxed LP and the original MILP model of L-shaped decomposition SP have the same optimal solution.*

Proof. Suppose we eliminate binary variables, formulating the problem as an LP. Simultaneous charging and discharging occur in the battery and tank ($b_{t\omega}^c, b_{t\omega}^d > 0$ and $h_{t\omega}^c, h_{t\omega}^d > 0$).

Applying the KKT optimality conditions, we modify (2) to (23a), with stationary conditions given in (23b) - (23e).

$$m_{t\omega_1}^d + m_{t\omega}^i + b_{t\omega}^d - l_t^e - b_{t\omega}^c - H/\eta^e (h_{t\omega}^c - h_{t\omega}^d + l_t^h) = 0 : \gamma_{t\omega} \quad \forall t, \forall \omega, \forall \omega_1 \in \omega \quad (23a)$$

$$-\gamma_{t\omega} + \eta^b \tau_{t\omega} + \underline{\tau}_{t\omega}^c - \bar{\tau}_{t\omega}^c = 0 \quad \forall t, \forall \omega \quad (23b)$$

$$\gamma_{t\omega} - \tau_{t\omega}/\eta^b + \underline{\tau}_{t\omega}^d - \bar{\tau}_{t\omega}^d = 0 \quad \forall t, \forall \omega \quad (23c)$$

$$-\gamma_{t\omega} H/\eta^e + \eta^h \nu_{t\omega} + \underline{\nu}_{t\omega}^c - \bar{\nu}_{t\omega}^c = 0 \quad \forall t, \forall \omega \quad (23d)$$

$$\gamma_{t\omega} H/\eta^e - \nu_{t\omega}/\eta^h + \underline{\nu}_{t\omega}^d - \bar{\nu}_{t\omega}^d = 0 \quad \forall t, \forall \omega \quad (23e)$$

Given the minimum charge and discharge capacities of zero, the Lagrangian multipliers $\underline{\tau}_{t\omega}^c$, $\underline{\tau}_{t\omega}^d$, $\underline{\nu}_{t\omega}^c$, and $\underline{\nu}_{t\omega}^d$ are all determined to be zero. Consequently, we obtain (24a) and (24b), leading to the derivation of (24c).

$$(\gamma_{t\omega} + \bar{\tau}_{t\omega}^c)/\eta^b = \eta^b (\gamma_{t\omega} - \bar{\tau}_{t\omega}^d) \quad \forall t, \forall \omega \quad (24a)$$

$$(\gamma_{t\omega} H/\eta^e + \bar{\nu}_{t\omega}^c)/\eta^h = \eta^h (\gamma_{t\omega} H/\eta^e - \bar{\nu}_{t\omega}^d) \quad (24b)$$

$$\forall t, \forall \omega$$

$$\gamma_{t\omega} (\eta^b - 1/\eta^b) + \gamma_{t\omega} H/\eta^e (\eta^h - 1/\eta^h) = \bar{\tau}_{t\omega}^c/\eta^b + \eta^b \bar{\tau}_{t\omega}^d + \bar{\nu}_{t\omega}^c/\eta^h + \eta^h \bar{\nu}_{t\omega}^d \quad \forall t, \forall \omega \quad (24c)$$

Assuming $b_{t\omega}^c, b_{t\omega}^d > 0$ and $h_{t\omega}^c, h_{t\omega}^d > 0$, the right-hand side of (24c) will be either 0 or strictly positive, while the left-hand side expression is negative. This contradiction implies that at least one of the variables $b_{t\omega}^c$ or $b_{t\omega}^d$ and $h_{t\omega}^c$ or $h_{t\omega}^d$ must be zero. \square

The L-shaped decomposition algorithm terminates upon meeting convergence criteria based on the relative gap or maximum iterations. The objective function of MP serves as the upper bound, while the total revenue minus DA expenses and SP objective value acts as the lower bound.

C. Improved L-shaped decomposition (ILSD) algorithm

To improve our L-shaped decomposition algorithm, we utilize warm start technique and innovative approach to tackle SP infeasibility. We also customize valid inequalities and employ cut disaggregation methods for enhanced efficiency. Details on implementing these strategies are provided in the subsequent section, along with a flowchart of our proposed algorithm (Fig. 6).

1) *Warm Start:* To accelerate our L-shaped implementation, we customized a warm start approach. In each iteration, MP uses information from the previous iteration's solution.

2) *Resolve Infeasibility:* When over-procuring power from the DA market renders SP infeasible, solutions include adding slack variables or feasibility cuts. However, slack variables lead to numerical instability, while feasibility cuts requires solving SP again to obtain the extreme ray, which is time-consuming. Therefore, we propose efficiently modifying (6a) to (25) to maintain feasibility, effectively penalizing power over-procurement for direct electric vehicle charging.

$$v_{t\omega}^e + b_{t\omega}^d \geq l_t^e \quad \forall t, \forall \omega \quad (25)$$

Lemma 2. *The relaxed constraint (25) is always tight at the optimal solution of optimization problem (1) - (11b).*

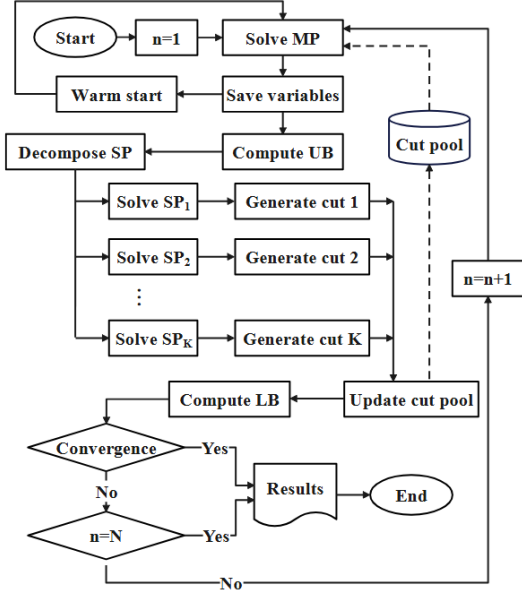


Fig. 6. Flowchart of the ILSD algorithm.

Proof. Let x^* be the optimal solution of (1) - (11b), and suppose there exists a set $(\hat{t}, \hat{\omega})$ such that $v_{\hat{t}\hat{\omega}}^{e*} + b_{\hat{t}\hat{\omega}}^{d*} > l_{\hat{t}}^e$:

$$\sum_t (v_{t\hat{\omega}}^{e*} + b_{t\hat{\omega}}^{d*}) > \sum_t l_t^e \quad \exists \hat{\omega} \quad (26)$$

By incorporating (2), (26) transforms into (27), where $\phi_{\hat{\omega}}^*$ is a positive auxiliary variable for (26).

$$\sum_t (m_{t\hat{\omega}_1}^{d*} + m_{t\hat{\omega}}^{i*}) = \sum_t (b_{t\hat{\omega}}^{c*} + e_{t\hat{\omega}}^{p*} - b_{t\hat{\omega}}^{d*} + l_t^e) + \phi_{\hat{\omega}}^* \quad \exists \hat{\omega}, \hat{\omega}_1 \in \hat{\omega} \quad (27)$$

The optimal objective function $\mathcal{F}(x^*)$ is given by (28), where $\phi_{\hat{\omega}}^*$ and $\sum_t (b_{t\hat{\omega}}^{c*} + e_{t\hat{\omega}}^{p*} - b_{t\hat{\omega}}^{d*} + l_t^e)$ are equal to $\phi_{\hat{\omega}}^{1*} + \phi_{\hat{\omega}}^{2*}$ and $\sum_t (\mu_{t\hat{\omega}}^{1*} + \mu_{t\hat{\omega}}^{2*})$, respectively.

$$\begin{aligned} \mathcal{F}(x^*) = & \sum_t (l_t^e p_t^e + l_t^h p_t^h) - \sum_{\substack{t', t \in t', \omega, \\ (\omega_1, \omega_2) \in \omega, \omega \neq \hat{\omega}}} \pi_{\omega} (m_{t\omega_1}^d \xi_{t'\omega_1}^d + \\ & m_{t\omega}^i \xi_{t\omega_2}^i) - \pi_{\hat{\omega}} (\phi_{\hat{\omega}}^{1*} \xi_{\hat{t}\hat{\omega}_1}^d + \sum_{t', t \in t', \hat{\omega}_1 \in \hat{\omega}} \mu_{t\hat{\omega}}^{1*} \xi_{t'\hat{\omega}_1}^d) - \\ & \pi_{\hat{\omega}} (\phi_{\hat{\omega}}^{2*} \xi_{\hat{t}\hat{\omega}_2}^i + \sum_{t', t \in t', \hat{\omega}_2 \in \hat{\omega}} \mu_{t\hat{\omega}}^{2*} \xi_{t'\hat{\omega}_2}^i) \end{aligned} \quad (28)$$

By tending $\phi_{\hat{\omega}}^*$ to zero, a new feasible solution x' is obtained where $v_{\hat{t}\hat{\omega}}^e + b_{\hat{t}\hat{\omega}}^d = l_{\hat{t}}^e$ and $\mathcal{F}(x')$ is as follows:

$$\mathcal{F}(x') = \mathcal{F}(x^*) + \pi_{\hat{\omega}} \xi_{\hat{t}\hat{\omega}_1}^d \phi_{\hat{\omega}}^{1*} + \pi_{\hat{\omega}} \xi_{\hat{t}\hat{\omega}_2}^i \phi_{\hat{\omega}}^{2*} \quad (29)$$

Since $\pi_{\hat{\omega}} \xi_{\hat{t}\hat{\omega}_1}^d \phi_{\hat{\omega}}^{1*} + \pi_{\hat{\omega}} \xi_{\hat{t}\hat{\omega}_2}^i \phi_{\hat{\omega}}^{2*} > 0$, then $\mathcal{F}(x') > \mathcal{F}(x^*)$, which is in contrast with the optimality of x^* . \square

Using constraint (25), we transform equation (22c) into constraint (30), expediting the L-shaped decomposition process.

$$\begin{aligned} \hat{m}_{nt\omega_1}^d - \hat{l}_{nt}^e & \geq -b_{t\omega}^d + b_{t\omega}^c + e_{t\omega}^p - m_{t\omega}^i : \lambda_{nt\omega} \\ \forall n, \forall t, \forall \omega, \forall \omega_1 \in \omega \end{aligned} \quad (30)$$

3) *Valid inequalities:* We introduce valid inequality (31) into the MP, which quickly removes infeasible solutions and accelerates convergence. This is necessary because our MP lacks constraints to prevent excessive power procurement from exceeding total demand, battery, and electrolyzer capacity.

$$m_{t\omega_1}^d \leq l_t^e + \bar{b}^c + \bar{e}^p \quad \forall t, \forall \omega_1 \quad (31)$$

4) *Disaggregation of optimality cut:* We adopt a practical approach to balance iteration quantity and cut production by generating several cuts during each iteration, transitioning from (21c) to (32a), where k denotes the number of cuts.

$$\begin{aligned} \alpha_k & \geq -\alpha_k \left(\hat{m}_{nt\omega_1}^d, \hat{l}_{nt}^e, \hat{l}_{nt}^h \right) + \sum_{t, \omega, \omega_1 \in \omega} \left[\left(\hat{m}_{nt\omega_1}^d - m_{t\omega_1}^d \right) \right. \\ & \left. \lambda_{nt\omega} + \left(\hat{l}_{nt}^e - l_t^e \right) \vartheta_{nt\omega} + \left(\hat{l}_{nt}^h - l_t^h \right) \varrho_{nt\omega} \right] \quad \forall n, \forall k \end{aligned} \quad (32a)$$

The flowchart illustrating all the aforementioned components involved in solving our problem is depicted in Fig. 7. Our approach combines several methods to address specific challenges in optimizing trading for Chargco in day-ahead and intraday markets. We have organized our approach into preprocessing and processing stages to provide a clearer overview. Each of these methods is specifically chosen to address unique challenges regarding market dynamics and operational characteristics.

• Preprocessing:

- *Generative Adversarial Networks (GANs):* We incorporate GANs to cluster scenarios, effectively managing the uncertainty in electricity prices without increasing computational complexity.
- *Random Forest:* We utilize random forest and linear regression to predict electricity and hydrogen load levels and their selling prices with accuracy. This step is crucial for ensuring robust trading decisions based on reliable data forecasts.
- *Linearization of Bilinear Terms:* To handle bilinear terms, we employ piecewise linearization with SOS2 variables. This allows us to approximate nonlinear relationships within the model, maintaining tractability.

• Processing:

- *Improved L-Shaped Decomposition (ILSD) Algorithm:* Our ILSD algorithm addresses computational challenges by dividing the problem into a master problem and sub-problem, sequentially optimizing trading strategies. It enhances efficiency through warm-start techniques, valid inequalities, and multiple-cuts generation, contributing to computational efficiency.
- *Optimal Bidding Curves:* The ILSD algorithm ultimately aids in obtaining optimal bidding curves for day-ahead and intraday market participation.

V. NUMERICAL EXPERIMENTS

We consider a Chargco participating in the DA and ID markets. The relevant information is provided in Table I.

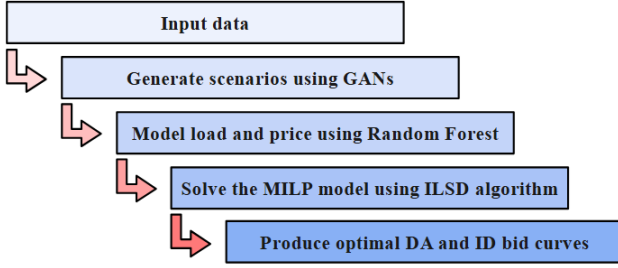


Fig. 7. Flowchart of our sequential steps.

TABLE I
REQUIRED INFORMATION OF DEVICES

Parameter	Value	Parameter	Value
η^b	0.85	η^h	0.9
$\underline{b}^l, \bar{b}^l$	0, 60 (kWh)	$\underline{h}^l, \bar{h}^l$	0, 20 (kg)
$\underline{b}^c, \bar{b}^c$	0, 15 (kW)	$\underline{h}^c, \bar{h}^c$	0, 5 (kg/h)
$\underline{b}^d, \bar{b}^d$	0, 15 (kW)	$\underline{h}^d, \bar{h}^d$	0, 5 (kg/h)
$\underline{e}^p, \bar{e}^p$	0, 1000 (kW)	η^e	0.8

A. Scenario generation

We evaluate our GANs model's ability to cluster electricity market prices by comparing the Cumulative Distribution Function (CDF) in Fig. 8. Using both GANs-generated scenarios and data from the German market provided by ENTSO-E [33], our analysis confirms a close match between the two CDFs, demonstrating accurate capture of electricity price dynamics. In stochastic programming, discrete distributions simplify extensive datasets for estimating probability distributions. Figure 9 illustrates this, discretizing a continuous PDF into four scenarios shown as rectangular bars.

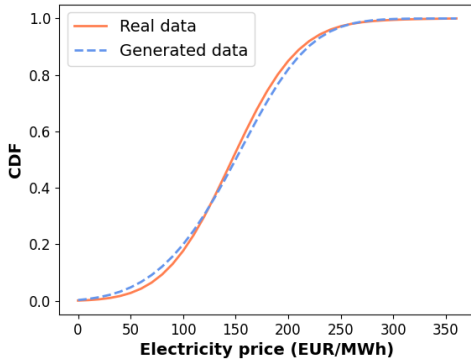


Fig. 8. CDF of the original dataset versus generated scenarios by GANs.

The application of random forest followed by linear regression offers insights into the dependency of electricity and hydrogen load levels on their price variations across different intervals. In Fig. 10, we illustrate the relationship between electricity load and price for a selected hour as an example.

B. Market analysis

Table II offers operational insights into the charging station dynamics, encompassing key parameters like energy levels,

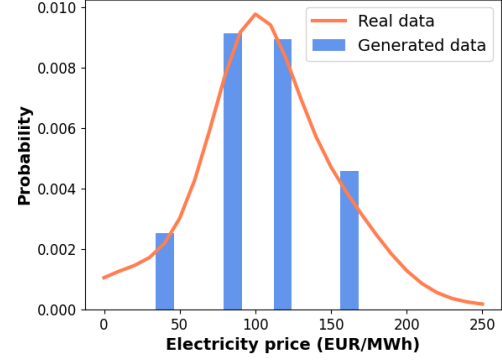


Fig. 9. PDF of the original dataset versus generated scenarios by GANs.

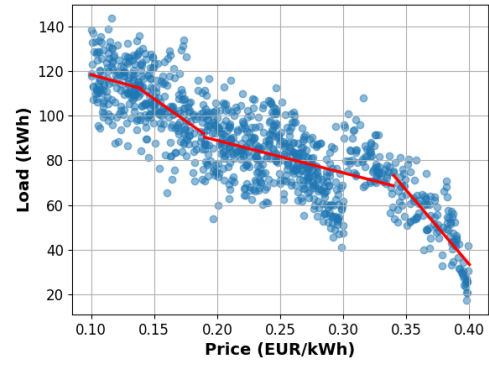


Fig. 10. Load and price relationship using random forest and linear regression.

loads, pricing trends, and purchases across different times. It enables analysis of how price changes influence operations. During low market prices, energy is stored, while during high prices, stored energy is discharged to minimize costs and enhance profitability by adapting to market conditions.

TABLE II
CHARGING STATION OPERATION

	t1	t2	t3	t4	t5	t6	t7	t8
DA price (EUR/MWh)	83.6	83.6	83.6	83.6	33.3	33.3	33.3	33.3
ID price (EUR/MWh)	102.6	88.7	80.3	61.9	15.0	82.9	74.3	20.0
Battery level (kWh)	-	-	-	-	12.8	-	-	-
Hydrogen level (kg)	-	-	-	-	4.5	4.5	-	-
Electricity load (kWh)	5.4	57.1	118.3	77.9	57.4	97.4	97.7	24.7
Hydrogen load (kg)	2.2	4.7	9.3	4.2	4.6	6.3	7.0	3.2
Electricity price (\$/kWh)	0.4	0.4	0.4	0.4	0.4	0.4	0.4	0.3
Hydrogen price (\$/kg)	10.8	13.0	14.0	14.0	13.0	14.0	14.0	10.6
DA purchase (kWh)	111	287	-	-	-	394	244	-
ID purchase (kWh)	-	-	576	282	543	-	-	185

Figure 11 illustrates the downward-sloping DA bidding curves (blue curve) for the Chargco for one selected hour. The red curve depicts the bidding curve when the downward-sloping condition is relaxed. Figure 12 shows ID bidding curves for one quarter-hour, reflecting two scenarios from the DA market. Different bidding curves in the ID market correspond to realized scenarios from the DA market, highlighting

sensitivity to DA market price fluctuations and emphasizing the need for accurate clustering of electricity market prices.

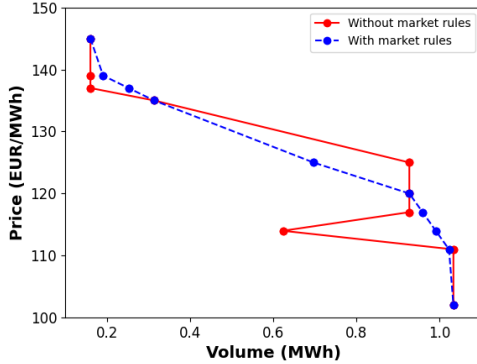


Fig. 11. Bidding curve without and with the consideration of market rule.

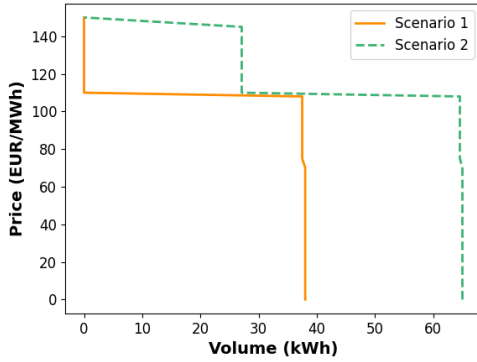


Fig. 12. ID bidding curves reflecting two DA market scenarios.

C. Computational discussions

Table III demonstrates that our ILSD algorithm successfully identifies the optimal solution with 2,300 scenarios over 96 discrete 15-minute intervals. In contrast, standard algorithms such as Benders decomposition and popular solvers like CPLEX and Gurobi fail to provide any solution, even for the linearized formulation. The convergence of our ILSD algorithm, illustrated in Fig. 13, demonstrates the effectiveness of our solution method for optimizing the proposed MILP model of Chargco trading.

TABLE III
THE COMPUTATIONAL RESULTS FOR OUR CASE STUDY

	Profit (EUR)	Time (h)	Iteration
CPLEX solver	*	*	*
Gurobi solver	*	*	*
Benders decomposition	*	*	*
Our ILSD	3740	4	162

VI. CONCLUSION

This paper presents a framework for optimizing a Chargco's participation in electricity auction markets. It employs a two-stage stochastic optimization framework, GANs for scenario

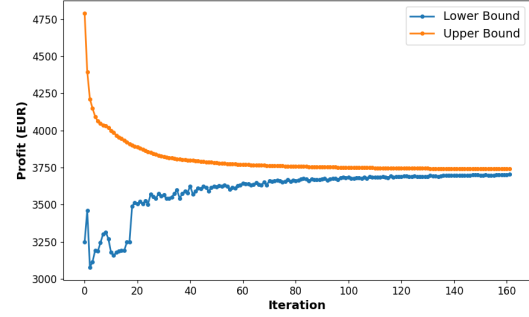


Fig. 13. Convergence procedure of our proposed ILSD algorithm.

clustering of electricity prices, and a hybrid approach using random forests and linear regression to depict load-price correlations. We linearize our MIQP using SOS2 variables and a max-affine function. We introduce an ILSD algorithm that effectively tackles L-shaped decomposition SP infeasibilities through a suggested procedure. It incorporates the integration of warm start, valid inequalities and the application of multiple-cuts generation, thereby streamlining computational complexity. We also reformulate the MILP model of L-shaped decomposition SP as an LP, validated by KKT conditions. Our optimization method ensures the maximum achievable profit for Chargco by efficiently managing resources, in environments with volatile electricity prices. It enables optimal and timely decision-making, significantly enhancing profitability and operational efficiency compared to approximation or heuristic methods.

ACKNOWLEDGMENTS

The research has been supported by the Czech Technical University in Prague, grant number SGS24/094/OHK5/2T/13, and the European Union under the project ROBOPROX (reg. no. CZ.02.01.01/00/22_008/0004590).

REFERENCES

- [1] P. V. Dahiwalé, Z. H. Rather, and I. Mitra, "A comprehensive review of smart charging strategies for electric vehicles and way forward," *IEEE Transactions on Intelligent Transportation Systems*, 2024.
- [2] H. Ritchie, "Cars, planes, trains: where do CO₂ emissions from transport come from?" *Our World in Data*, 2020, <https://ourworldindata.org/co2-emissions-from-transport>.
- [3] F. Sohrabi, M. Rohaninejad, M. R. Hesamzadeh, and J. Bemš, "Optimal trading of a hybrid electric, hydrogen and gas fueling station in day-ahead and intra-day markets: Modeling aspect," in *International Conference on Operations Research*. Springer, 2022, pp. 289–295.
- [4] Z. M. Shoja, M. A. Mirzaei, H. Seyedi, and K. Zare, "Sustainable energy supply of electric vehicle charging parks and hydrogen refueling stations integrated in local energy systems under a risk-averse optimization strategy," *Journal of Energy Storage*, vol. 55, p. 105633, 2022.
- [5] P. G. Panah, M. Bornapour, R. Hemmati, and J. M. Guerrero, "Charging station stochastic programming for hydrogen/battery electric buses using multi-criteria crow search algorithm," *Renewable and Sustainable Energy Reviews*, vol. 144, p. 111046, 2021.
- [6] X. Xu, W. Hu, D. Cao, Q. Huang, W. Liu, M. Z. Jacobson, and Z. Chen, "Optimal operational strategy for an offgrid hybrid hydrogen/electricity refueling station powered by solar photovoltaics," *Journal of Power Sources*, vol. 451, p. 227810, 2020.

- [7] F. Sohrabi, M. Rohaninejad, M. R. Hesamzadeh, and J. Bemš, “Coordinated bidding of multi-product charging station in electricity markets using rolling planning and sample average approximation,” *International Journal of Electrical Power & Energy Systems*, vol. 146, p. 108786, 2023.
- [8] X. Xu, W. Hu, W. Liu, Y. Du, Q. Huang, and Z. Chen, “Robust energy management for an on-grid hybrid hydrogen refueling and battery swapping station based on renewable energy,” *Journal of Cleaner Production*, vol. 331, p. 129954, 2022.
- [9] T. Sriyakul and K. Jermsittiparsert, “Risk-constrained design of autonomous hybrid refueling station for hydrogen and electric vehicles using information gap decision theory,” *International Journal of Hydrogen Energy*, vol. 46, no. 2, pp. 1682–1693, 2021.
- [10] G. Guo and Y. Gong, “Energy management of intelligent solar parking lot with ev charging and fcev refueling based on deep reinforcement learning,” *International Journal of Electrical Power & Energy Systems*, vol. 140, p. 108061, 2022.
- [11] Y. Elmasry, I. B. Mansir, Z. Abubakar, A. Ali, S. Aliyu, and K. Almamun, “Electricity-hydrogen nexus integrated with multi-level hydrogen storage, solar pv site, and electric-fuelcell car charging stations,” *International Journal of Hydrogen Energy*, 2024.
- [12] P. Cai, Y. Mi, S. Ma, H. Li, D. Li, and P. Wang, “Hierarchical game for integrated energy system and electricity-hydrogen hybrid charging station under distributionally robust optimization,” *Energy*, vol. 283, p. 128471, 2023.
- [13] S. M. Dastjerdi, Z. M. Mosammam, P. Ahmadi, and E. Houshfar, “Transient analysis and optimization of an off-grid hydrogen and electric vehicle charging station with temporary residences,” *Sustainable Cities and Society*, vol. 97, p. 104742, 2023.
- [14] A. Mansour-Saatloo, R. Ebadi, M. A. Mirzaei, K. Zare, B. Mohammadi-Ivatloo, M. Marzband, and A. Anvari-Moghaddam, “Multi-objective igdt-based scheduling of low-carbon multi-energy microgrids integrated with hydrogen refueling stations and electric vehicle parking lots,” *Sustainable Cities and Society*, vol. 74, p. 103197, 2021.
- [15] A. Çiçek, “Optimal operation of an all-in-one ev station with photovoltaic system including charging, battery swapping and hydrogen refueling,” *International Journal of Hydrogen Energy*, vol. 47, no. 76, pp. 32405–32424, 2022.
- [16] M. Schröder, Z. Abdin, and W. Mérida, “Optimization of distributed energy resources for electric vehicle charging and fuel cell vehicle refueling,” *Applied energy*, vol. 277, p. 115562, 2020.
- [17] M. Narajewski and F. Ziel, “Optimal bidding in hourly and quarter-hourly electricity price auctions: Trading large volumes of power with market impact and transaction costs,” *Energy Economics*, vol. 110, p. 105974, 2022.
- [18] F. Ocker and V. Jaenisch, “The way towards european electricity intraday auctions—status quo and future developments,” *Energy policy*, vol. 145, p. 111731, 2020.
- [19] Y. Chen, Y. Wang, D. Kirschen, and B. Zhang, “Model-free renewable scenario generation using generative adversarial networks,” *IEEE Transactions on Power Systems*, vol. 33, no. 3, pp. 3265–3275, 2018.
- [20] I. Goodfellow, J. Pouget-Abadie, M. Mirza, B. Xu, D. Warde-Farley, S. Ozair, A. Courville, and Y. Bengio, “Generative adversarial nets,” *Advances in neural information processing systems*, vol. 27, 2014.
- [21] T. Deng, H. Yan, and Y.-J. Li, “Learning to boost bottom-up fixation prediction in driving environments via random forest,” *IEEE Transactions on Intelligent Transportation Systems*, vol. 19, no. 9, pp. 3059–3067, 2017.
- [22] S. A. Shevchik, F. Saeidi, B. Meylan, and K. Wasmer, “Prediction of failure in lubricated surfaces using acoustic time–frequency features and random forest algorithm,” *IEEE Transactions on Industrial Informatics*, vol. 13, no. 4, pp. 1541–1553, 2016.
- [23] A. Jahangiri and H. A. Rakha, “Applying machine learning techniques to transportation mode recognition using mobile phone sensor data,” *IEEE transactions on intelligent transportation systems*, vol. 16, no. 5, pp. 2406–2417, 2015.
- [24] S. S. Fazeli, S. Venkatachalam, R. B. Chinnam, and A. Murat, “Two-stage stochastic choice modeling approach for electric vehicle charging station network design in urban communities,” *IEEE Transactions on Intelligent Transportation Systems*, vol. 22, no. 5, pp. 3038–3053, 2020.
- [25] S. Y. Derakhshandeh, A. Ghiasian, and M. A. Masoum, “A new time-decoupled framework for pevs charging and scheduling in industrial microgrids,” *IEEE Transactions on Smart Grid*, vol. 10, no. 1, pp. 568–577, 2017.
- [26] “EPEX SPOT,” <https://www.epexspot.com/en>, accessed: March 22, 2024.
- [27] J. Wang, Z. Zhao, G. Liu, and H. Xu, “A robust optimization approach of well placement for doublet in heterogeneous geothermal reservoirs using random forest technique and genetic algorithm,” *Energy*, vol. 254, p. 124427, 2022.
- [28] B. Yang, K. Inoue, Z. Yan, Z. Wang, S. Kitazaki, and K. Nakano, “Influences of level 2 automated driving on driver behaviors: A comparison with manual driving,” *IEEE Transactions on Intelligent Transportation Systems*, 2023.
- [29] Home - Keras Documentation. <https://keras.io/>. [Accessed: 2023].
- [30] Tensorflow. <https://www.tensorflow.org/>. [Accessed: 2023].
- [31] J. Ashraf, A. D. Bakhshi, N. Moustafa, H. Khurshid, A. Javed, and A. Beheshti, “Novel deep learning-enabled lstm autoencoder architecture for discovering anomalous events from intelligent transportation systems,” *IEEE Transactions on Intelligent Transportation Systems*, vol. 22, no. 7, pp. 4507–4518, 2020.
- [32] P. Duan, G. Mao, J. Kang, and B. Huang, “Estimation of link travel time distribution with limited traffic detectors,” *IEEE Transactions on Intelligent Transportation Systems*, vol. 21, no. 9, pp. 3730–3743, 2019.
- [33] Entso-e. <https://www.entsoe.eu/>. [Accessed: 2023].